JOURNAL OF SPACECRAFT AND ROCKETS
Vol. 38, No. 3, May–June 2001

Near-Field Measurement and Modeling Results for Flight-Type Arcjet: Hydrogen Atom

Mark W. Crofton* and Teresa A. Moore†
The Aerospace Corporation, Los Angeles, California 90009
Iain D. Boyd‡
University of Michigan, Ann Arbor, Michigan 48109-2140
Ideo Masuda§
National Space Development Agency, Ibaraki 305-8505, Japan
and
Yoshifumi Gotoh¶
Mitsubishi Electric Corporation, Kanagawa 247, Japan

Hydrogen atoms were probed in the near-field plume of a 1.8-kW flight-type arcjet thruster, using two-photon laser-induced fluorescence. The arcjet was operated on an N_2/H_2 gas mix simulating hydrazine decomposition products. The velocity distributions of H atoms were used to obtain their translational temperatures. Comparisons of the laser-induced fluorescence signal intensity, radial linewidth, and derived density distribution with direct simulation Monte Carlo results were in good agreement except near the nozzle exit plane. A relatively weak signal was observed near the exit plane, while the maximum signal was unexpectedly obtained 0.8 cm downstream. Fluorescence quenching, linewidth variation, and self-absorption effects are proposed to account for most of the discrepancy in signal intensity. The results improve the knowledge of near-field flow parameters for the arcjet and ultimately enhance the accuracy and understanding of predicted plume impingement torques and other arcjet plume phenomenology on spacecraft.

Nomenclature

a	=	Gaussian normalization parameter, dimensionless
b	=	Gaussian linewidth parameter, cm^{-1}
c	=	speed of light
E_{kg}	=	transition energy between states k and g
e	=	elementary charge
f	=	oscillator strength, dimensionless
g	=	ground quantum state
$g(\nu)$	=	Gaussian line shape function, dimensionless
$\hbar$	=	Planck's constant divided by 2π
I_ν	=	intensity of photon flux at frequency ν
k	=	intermediate quantum state
k_ν	=	absorption coefficient at frequency ν
L	=	absorption pathlength
l	=	final quantum state
M	=	species molar mass
m	=	electron mass
N_i	=	density of species i, cm^{-3}
r	=	radial coordinate, cm
T	=	temperature, K
z	=	axial coordinate, cm
$\Delta\nu_D$	=	Doppler full-width-half-maximum, cm^{-1}
δ	=	two-photon absorptivity
ε_0	=	permittivity constant
$\hat{\varepsilon}_1$	=	polarization vector for photon 1
$\hat{\varepsilon}_2$	=	polarization vector for photon 2
$\boldsymbol{\mu}_{op}$	=	electric dipole operator
ν	=	frequency
ν_0	=	center frequency
σ	=	absorption cross section
ω	=	angular frequency

Subscripts

D	=	Doppler
L	=	laser
S	=	Stark effect
SA	=	self-absorption

Received 9 June 2000; revision received 2 February 2001; accepted for publication 2 February 2001.

*Research Scientist, Laboratory Operations, Propulsion Science and Experimental Mechanics Department, M5-754, P.O. Box 92957. Member AIAA.

†Member of Technical Staff, Laboratory Operations, Propulsion Science and Experimental Mechanics Department, M5-754, P.O. Box 92957.

‡Associate Professor, Department of Aerospace Engineering, 1320 Beal Avenue. Senior Member AIAA.

§Assistant Senior Engineer, Data Relay Test Satellite Project Team, 2-1-1 Sengen, Tsukuba.

¶Senior Engineer, Space Systems Department, 325, Kamimachiya Kamakura.

Introduction

NORTH–SOUTH stationkeeping for the data relay test satellites (DRTS) developed for launch around 2001 and the succeeding year will be provided by MR-509A/B hydrazine arcjet thrusters.[1] Despite the successful operation of PRIMEX Aerospace Corporation (PAC) arcjets on several U.S. satellites,[2] little quantitative information has been readily available about the thruster impact on satellites of arbitrary configuration. To rectify this situation for the DRTS case, experimental measurements were performed and coupled with theoretical analyses. The measurement program resulted in the first laser-induced fluorescence and mass spectrometric studies for a flight-type arcjet thruster. A portion of the experimental work concerned with the measurement of near-field parameters is described in this report.

Near-field plume data are valuable for the understanding of the arcjet flow and performance properties. The term near-field is intended to designate the volume within the first several centimeters downstream from the nozzle exit plane, a region in which most parameters are changing rapidly.

The study of the arcjet-induced effects of spacecraft plume impingement and torquing, as well as contamination and thermal loading, is best accomplished via direct simulation Monte Carlo (DSMC) calculations. Code validation can be achieved via data comparisons and improvements in computational accuracy by incorporating experimental results into the modeling analysis (where feasible, and

provided that those results are accurate).[3] In the present study, an existing DSMC code that was previously validated on a reacting arcjet flow of H_2 was applied to a reacting flow of H_2 and N_2.

The H atom served as a probe species to study arcjet plume properties. The main quantities studied were kinetic temperature and density distribution. Previous arcjet studies[4–7] have examined properties of this species, which has a high number density in the MR-509 plume. To obtain average properties for H atoms, as opposed to average properties of individual excited states, the lower state of the excitation was chosen to involve the ground electronic state. Only the ground state population is a good approximation of total species density. Kinetic temperature is state specific in principle, but in practice no differences are usually detected. Ground-state probing of the H atom had not previously been performed for a hydrazine or simulated-hydrazine arcjet.

The hydrogen atom is one of the most abundant species in the near field of the hydrazine arcjet plume, but is a minor momentum carrier because of its low atomic weight. Hydrogen atoms emerge from the arc excitation region with the highest velocity, both directed and random, because they have lower mass than other arcjet species. The directed and random velocity of H atoms is substantially reduced in the plume expansion by collisions with relatively massive partners. Separation of H from species such as N_2 and NH is inevitable because of its relatively high perpendicular and parallel velocity components, coupled with scattering away from the plume center by collisions with heavier species. Comparison with the companion paper to the present study illustrates the species variability in near-field parameters.[8] Density, peak axial velocity, and kinetic, rotational, and vibrational temperatures were obtained for the NH molecule, and compared to DSMC results. Agreement between theory and experiment was generally good for that species, despite a more narrow velocity distribution function and relatively low density.

Two fundamental discrepancies between theoretical and experimental results for the hydrogen arcjet plume have been recently resolved by revised data interpretation or new experimental data, both vindicating theory. In one case, the experimental linewidth of the H atom Balmer alpha (H_α) transition was far more broad than the DSMC calculation predicted,[7] and in the other, the experimentally obtained dissociation fraction of H_2 was several times higher than the DSMC result.[6,8] These cases illustrate the increasing value of the DSMC method to aid the interpretation of experimental data obtained under complex circumstances and to fill data and knowledge gaps that are not readily closed by a purely experimental approach.

Experimental Setup

Test Facility and Arcjet Operation

The experimental test chamber was 5.5 m in length with a diameter of 2.4 m. Test chamber vacuum was maintained by 16 VHS-400 diffusion pumps. During thruster operation at the nominal flow rate of 46.4 mg/s, test chamber background pressure was maintained below 1×10^{-3} torr.

The thruster was mounted on a computer-controlled four-axis positioning system. The arcjet nozzle was aligned with the long axis of the test chamber and remained there. The vertical position of the arcjet was similarly fixed for the duration of the measurements. Two-axis positioning was performed in the axial and radial directions to explore the spatial dependence of near-field parameters.

Electrical power of 1.8 kW was supplied at 80-V dc to a power conditioning unit (PCU) provided by PAC. Power was supplied at 28-V dc to operate the protection and control electronics, which were also provided by PAC. A flight-model PCU for DRTS, which would have required an input voltage of 33–51.5 V dc (Ref. 1), was not used.

A computer-controlled data acquisition and control system was supplied by The Aerospace Corporation and set up to satisfy PAC specifications regarding arcjet operating limits. Arcjet operating voltage, current, inlet pressure, and flow rates were monitored at all times, and an automatic shutdown would have occurred had any process limit been exceeded during normal operations. Typical recorded parameters at the 46.4-mg/s nominal operating point at which all H atom data were obtained are 46.4-mg/s flow rate, 0.8-mtorr background pressure, 109.7-V arc voltage, 15.1-A arc current, 1.66-kW input power, 235-mN thrust [estimated from flight qualification data of Ref. 9, with 2% reduction for use of simulated N_2H_4 (2:1 mix of H_2, N_2)], and 517-s I_{sp} (also estimated from Ref. 9). These quantities were reduced by 2% based on previous arcjet performance measurements comparing simulated N_2H_4 (2:1 mix of H_2:N_2) at ambient inlet temperature to catalytic decomposition of liquid N_2H_4 (Ref. 10). In practice, voltage and current levels varied somewhat, but the power conditioner kept arcjet input power constant at 1.66 kW.

Laser-Induced Fluorescence

Laser-induced fluorescence (LIF) is the preferred means of obtaining the near-field parameters discussed in this report. The technique offers high spatial resolution together with high sensitivity and results that are acceptable from a quantitative standpoint. Submillimeter spatial resolution was achieved in the present study. This is a requirement in the near field because the arcjet nozzle width at the exit plane is on the order of a centimeter. Sensitivity is a factor at the existing species densities, which range from 10^{12} to 10^{16} cm^{-3} in the probed region. The H atom ground state was probed via a two-photon LIF technique because a one-photon approach can only probe excited states (unless the wavelength is in the XUV spectral region,[4] making photon generation and fluorescence detection difficult and limiting spatial resolution). Excited state properties, particularly density, do not always replicate ground-state distributions.

In the case of simultaneous absorption of two photons, the absorption cross section derived from perturbation theory is[11]

$$\sigma = [(2\pi)^2/\hbar c^2] I\omega |M_{lg}|^2 g(\nu) \tag{1}$$

where M_{lg} is the two-quantum matrix element that may be written as

$$M_{lg}(\omega) = 2 \sum_k \frac{\langle l|\hat{\varepsilon}_1 \cdot \boldsymbol{\mu}_{\text{op}}|k\rangle \langle k|\hat{\varepsilon}_2 \cdot \boldsymbol{\mu}_{\text{op}}|g\rangle}{E_{kg} - \hbar\omega} \tag{2}$$

For a strong two-photon transition, the ratio σ/I is $\approx 10^{-30}$ cm^4/W. At low light intensities, single-photon absorption may be written in differential form as

$$-\mathrm{d}I = \sigma I N_i \, \mathrm{d}x \tag{3}$$

where dx makes an infinitesimal contribution to L. When multiple-photon absorption is included, the cross section may be expressed as

$$\sigma_{\text{tot}} = \sigma + 2I\delta + \cdots \tag{4}$$

where δ is the two-photon absorptivity, and for two-photon absorption Eq. (3) becomes

$$-\mathrm{d}I = 2\delta I^2 N_i \, \mathrm{d}x \tag{5}$$

A typical two-photon cross section $I\delta$ is about 7 orders of magnitude smaller than a one-photon cross section. For molecules with a center of symmetry, one-photon electric dipole transitions are allowed where two-photon transitions are forbidden and vice versa. This situation does not apply to the hydrogen atom, which is why it is possible to readily observe the L_β transition in one- or two-photon absorption as well as one-photon emission.

Quenching of excited states, usually a problem at high gas densities, may occur as a result of collisions with partners in other quantum states. For the arcjet, the sum of species densities at the nozzle exit plane is about 1.0×10^{16} cm^{-3}. In LIF measurements, if the upper state lifetime is much shorter than the interval between quenching collisions, quenching effects can be neglected. This is the case for the $n = 3\ ^2D_{3/2,5/2}$ levels of the hydrogen atom in most regions of the plume expansion because the zero-pressure lifetime is about 16 ns. Quenching effects are to be expected inside the nozzle.

A tunable Continuum dye laser operating on R640 dye was pumped by the 532-nm beam of a 10-Hz doubled YAG laser.

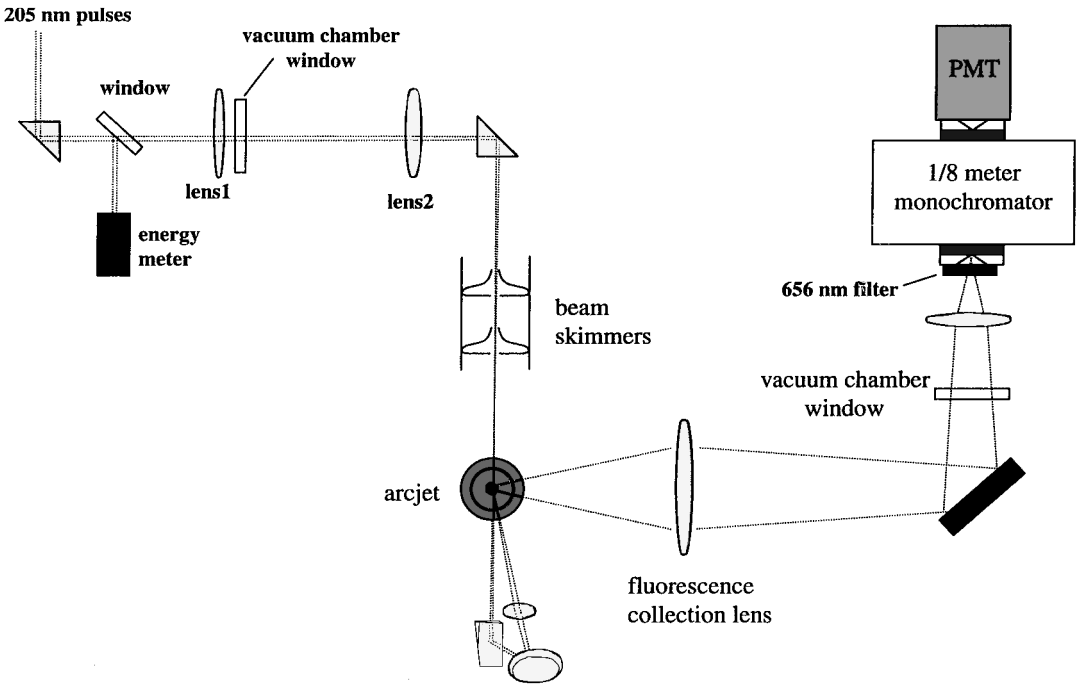

Fig. 1 Experimental setup.

The dye laser output at 615 nm was doubled in a KDP crystal, generating up to a 20-mJ/6-ns pulse at 307.5 nm. The crystal was tuned via a tracking circuit to maintain maximum output despite temperature drifts and frequency tuning. The H atom two-photon excitation wavelength of 205 nm was generated by mixing the doubled dye laser output (307.5 nm) with the fundamental (615 nm), each of appropriate polarization, in a β–$BaBO_4$ crystal mounted on a manual angle-tuning translation stage. Pulse energy up to 1.0 mJ was obtainable at 205 nm, but the level was maintained at 400–500 μJ using the variable energy output of the YAG laser.

After elevation to the appropriate height for entry into the vacuum chamber, the laser beam passed through a lens of 2-m focal length and a vacuum window. The beam was more tightly focused inside the chamber by a second lens of 35-cm focal length, located about 0.8 m from the first lens. The beam was then passed through the arcjet plume perpendicular to the thrust axis. A schematic diagram of the experimental setup is given in Fig. 1. To obtain an axial velocity measurement, an optic placed below the thruster steered the beam to a second optic sitting downstream and below the thrust axis. The latter optic steered the beam to intersect the plume at an angle of $\approx$40 deg with respect to the thrust axis and in the correct location to be aligned with the fluorescence collection optics. The laser beam was strongly focused to probe the H atom because of the cross section dependence on laser intensity [see Eq. (4)]. Fluorescence was collected by a 5-cm-diam MgF_2 lens placed 18 cm away from the arcjet centerline. The slowly converging fluorescence beam was transmitted over a distance of 1.2 m to a reflector that steered it through an LiF window into the external environment, where it passed through a 10-nm bandpass filter and entered a $\frac{1}{8}$-m monochromator. Detection was accomplished by means of a Hamamatsu R955 photomultipler tube attached at the monochromator exit. A boxcar amplifier was used to integrate the signal. Alignment of the collection optics was accomplished using an HeNe laser propagated back from the monochromator entrance or scattered light from the probe laser at the location of interest.

The beam diameter at the focal point was estimated to be on the order of 100 μm. At the arcjet, the pulse energy was 150–200 μJ, with shot-to-shot fluctuations $\leq$20%. Average power was constant to better than 3% while measuring peak signal profiles and better than 20% for lineshape measurements. The observed signal depended approximately on pulse energy squared, based on a two-point signal comparison at widely different pulse energies.

The laser pulse energy generating the H atom fluorescence was recorded together with the fluorescence signal by computer. Typically 30 shots were averaged per data point, after normalizing each according to the square of pulse energy. The normalization procedure was very successful in reducing the experimental noise level, confirming the energy-squared dependence of the signal.

Lineshapes were recorded by stepping the dye laser frequency, collecting signal for a suitable period, and repeating over the full range of the transition. Fundamental frequencies were obtained in vacuum wave numbers using a pulsed wavemeter, normally accurate to about 0.01 cm^{-1}. The wavemeter was automatically calibrated at intervals with an internal helium–neon laser, but was subject to minor drifting behavior between calibrations, which occasionally resulted in absolute readout errors of up to 0.03 cm^{-1}. Relative error was about 0.01 cm^{-1} for the recording of individual lineshapes. The low noise level of the lineshape data is consistent with this figure.

Lineshapes were typically fitted with a three parameter Gaussian function,

$$g(\nu) = a \exp\left\{-\tfrac{1}{2}[(\nu - \nu_0)/b]^2\right\} \tag{6}$$

In many cases the transition center frequency was fixed, but the linewidth parameter and peak height were always variables. These parameters normally showed little dependence on whether the center frequency was fixed. The small residual baseline present in the experimental measurements was subtracted before fitting. The linewidth is determined largely by Doppler broadening and laser linewidth, although Stark- and self-broadening are issues near the arcjet exit plane. The Doppler width is determined by the Maxwell–Boltzmann distribution and is related to temperature by

$$\Delta\nu_D = 2\sqrt{2\ln 2}\, b_D = 7.162 \times 10^{-7} \nu_0 \sqrt{T/M} \tag{7}$$

where

$$b_D \cong \sqrt{b^2 - b_L^2 - b_S^2 - b_{\mathrm{SA}}^2} \tag{8}$$

Because Stark broadening and self-broadening do not give rise to a Gaussian lineshape, Eq. (8) is an approximation applicable where b_S and b_{SA} are effective widths and $b_{\mathrm{SA}}^2, b_S^2 \ll (b_D^2 + b_L^2)$. The translational temperature (degrees Kelvin) may be expressed as

$$T = 1.0811 \times 10^{13} \left(M/\nu_0^2\right) b_D^2 \tag{9}$$

Table 1 Hydrogen atom fine and hyperfine structure (adapted from Ref. 12)

State[a]	Energy,[b] MHz	Hyperfine energy, MHz	ω, 10^9 s^{-1}[c]	Γ, 10^9 s^{-1}[d]
$3\,^2S_{1/2}$ $(F=0)$	0.0	−39.457	0.0	0.0063
$3\,^2P_{3/2}$ $(F=1)$	2935.191	−4.380	18.66274	0.1897
$3\,^2P_{1/2}$ $(F=1)$	−314.898	+4.382	−1.70311	0.1897
$3\,^2D_{5/2}$ $(F=2)$	4013.197	−1.577	25.45367	0.0647
$3\,^2D_{3/2}$ $(F=2)$	2929.859	+1.577	18.66668	0.0647

[a] S state taken as the origin. [b] Neglects hyerfine splitting. [c] Energy with hyperfine splitting included. [d] Inverse lifetime.

where M is in atomic mass units and ν_0 is cm^{-1}. The laser full-width-half-maximum (FWHM) linewidth at the fundamental output of the dye laser (565–680 nm) was assumed to be 0.07 cm^{-1} and Gaussian, in approximate agreement with the dye laser specifications and the linewidth suggested by a rough one-time analysis using the wavemeter.

Information about the $n=3$ upper states of the hydrogen atom is detailed in Table 1.[12] The allowed upper states of the two-photon absorption, which originates from the $n=1\ ^2S_{1/2}$ ground state, are $n=3\ ^2D_{3/2,5/2}$ and $^2S_{1/2}$. The transition intensity is about seven times greater for the ^2D upper levels than for $^2S_{1/2}$. The fluorescence lifetime of $^2S_{1/2}$ is an order of magnitude greater. To obtain good signal to noise ratio on the H_α transition despite the intense continuous background from the arcjet plume, the fluorescence detection gate width was set to about 13 ns. As a result, an insignificant amount of signal involving the $n=3\ ^2S_{1/2}$ level was collected.

For axial and radial measurements of the LIF signal, the laser frequency was positioned at the center of the transition lineshape. Some variation occurs in the lineshape as a function of the radial and axial coordinate, and therefore, the observed raw signal is only an approximate indicator of relative H atom density. To obtain accurate density information, it is necessary to know the lineshape as well as peak signal so that integrated signal strength can be obtained. For these measurements, as for lineshapes, error levels of individual data points can be estimated according to their deviations from the fitted curve. The typical error is substantially less than in the previous H-atom study.[6]

Numerical Approach

The flow inside the hydrazine arcjet is characterized by relatively low densities and very high temperatures. The Knudsen number (ratio of mean free path to boundary-layer scale) of the nozzle flow varies from about 0.001 at the nozzle throat to about 0.1 at the nozzle exit plane. These values indicate that the flow will be in a state of thermochemical nonequilibrium. At the same time, on the flow axis near to the arc constriction, the ionization level can be as high as 40% (Ref. 13).

These conditions place a heavy demand on attempts to perform accurate numerical simulations of the arcjet flow. At PAC a continuum-based computer code called KARNAC has been developed for computing arcjet flows. The code has performed very well in detail for hydrogen arcjet flows.[14] The accuracy of the code for hydrazine flows is less clear. There are several physical limitations of the KARNAC code. First, all energy modes are assumed to be in equilibrium. An equilibrium condition precludes the possibility of freezing of the vibrational and rotational energy modes of the molecular species in the flow (N_2 and H_2). Residual energy in such modes, however, is known to be a significant loss mechanism for arcjets. Second, by the time a Knudsen number of 0.1 is reached, the physical basis of the Navier–Stokes equations of fluid mechanics is no longer valid. Finally, because there is no thermal nonequilibrium included, important physical phenomena, such as vibration–dissociation coupling, are missing.

Although we are primarily interested in analysis of the arcjet plume, for the reasons listed earlier, a more detailed analysis of the nozzle flow is also merited. In the present study, the DSMC method[15] is employed to compute both the nozzle and plume flows in a single simulation. The DSMC technique is a kinetic-based method that follows the motions and collisions of test particles in the physical domain of interest. By time averaging the particle quantities throughout the computational domain, average properties such as density, velocity, and temperature are computed as moments of the particle distribution function. In the present study, the velocity distribution functions themselves are of interest. This is straightforward using the DSMC technique, but requires the computations to be performed over long periods to reduce statistical fluctuations.

The nozzle flow is begun just downstream of the constrictor in a region of the flow that is in the continuum regime. A startline for the DSMC computation is obtained from a solution generated by KARNAC and provided by PAC. The DSMC code includes the following physical phenomena: 1) multispecies flow (H_2, H, H^+, e, N_2, and N); 2) rotational and vibrational relaxation; 3) dissociation (with vibration coupling), ionization, and recombination reactions; and 4) ohmic heating. The code is described in detail in Ref. 13 and has been extensively validated against experimental data for hydrogen arcjets.[16]

In terms of boundary conditions, the nozzle wall is treated as being diffuse with full accommodation of all energy modes to a fixed temperature of 1400 K. For the plume expansion, the experimentally determined backpressure of 0.113 Pa is imposed. The analysis is performed for the nominal operating case of a flow rate of 46.4 mg/s and a power input to the arcjet of 1660 W.

Good spatial accuracy of the DSMC technique requires that cell sizes be on the order of a local mean free path with a minimum of 10 particles per cell. To meet these criteria, a computational grid of 500 by 70 cells is employed together with a total number of 350,000 particles.

If the computational statistics approximate a Poisson distribution, the statistical error will decay as (sample size)$^{-1/2}$. In computing the velocity and density distributions, the code was run for a sufficient period to reduce Poisson statistical error to levels below 1%. Actual errors may be much larger than 1% if the Poisson distribution does not apply or if sizable errors exist in the KARNAC output because KARNAC provides the starting point for the DSMC calculation. Comparisons with experimental data are, therefore, important for code validation.

Results and Discussion

Lineshapes, Broadening Mechanisms, and Temperature

The fitted lineshapes obtained at several coordinates along the plume axis are plotted in Figs. 2 and 3. The DSMC lineshape, computed by transforming the velocity distribution function according to the Doppler shift, is given for comparison in each case. No laser line broadening was added to the DSMC result. The FWHM linewidths are plotted in Fig. 4 for the DSMC results and for the Gaussian fits to the experimental data.

The Doppler-free two-photon absorption spectrum of the $n=3\leftarrow n=1$ transition[17,18] provides definitive relative intensities and peak positions. The spectrum shows that, whereas the relative intensities and peak positions do depend on electric field strength, the intense peaks remain within a 0.05-cm^{-1} band. Because the frequency plotted in the lineshape (see Figs. 2 and 3) is the dye laser fundamental frequency, corresponding to the two-photon frequency sum divided by 6, the corresponding region in the plots spans less than 0.01 cm^{-1}. The energy separation of the most relevant levels for normal two-photon absorption, the D states, is only 1.1 GHz or 0.036 cm^{-1}, also insignificant compared to the observed linewidth. Fine structure splitting has, therefore, been ignored in the lineshape fitting.

All of the lineshapes in Figs. 2 and 3 are well fitted by a Gaussian function, indicating that broadening mechanisms such as Stark effect and self-absorption, which add non-Gaussian character, are small compared to Doppler broadening. However, the experimental linewidth is noticeably broadened near the nozzle exit plane, with respect to the DSMC prediction for Doppler width (see Fig. 4) and a previous measurement on the NASA 1-kW hydrogen arcjet.[6] For the latter, theory and experiment were in close agreement. The quality of the radial linewidth comparison gives a degree of confidence in the DSMC prediction of axial Doppler width (see Fig. 4), despite a lack of LIF data for comparison.

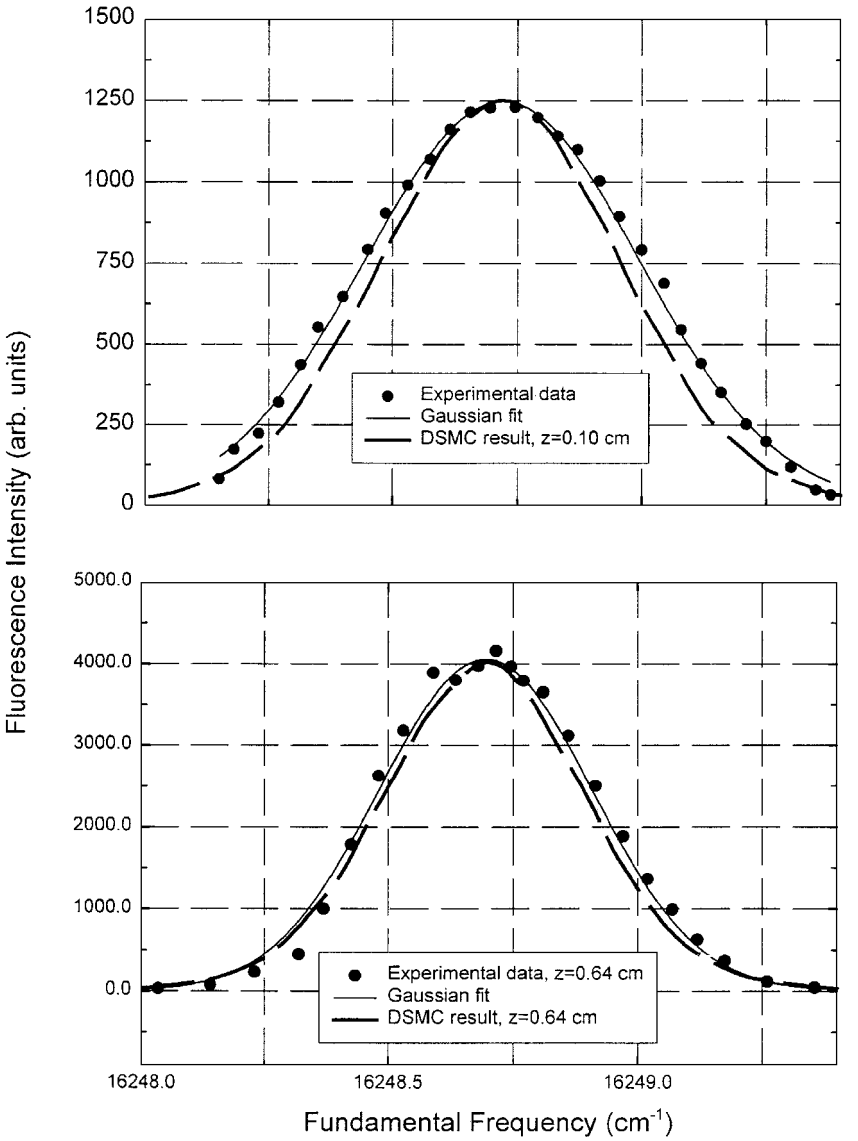

Fig. 2 Lineshapes on plume centerline at 1.0 (upper panel) and 6.4 (lower panel) ± 0.3 mm downstream from exit plane; laser beam intersected the plume perpendicular to the thrust axis.

The degeneracy of same n, different l levels of the hydrogen atom, split only by spin and relativity effects, gives rise to a first-order Stark effect. However, lines with odd Δn, such as H_α and H_γ and L_α and L_γ, have a central Stark component that is unshifted in first order, whereas no such central component exists for even Δn transitions such as H_β or L_β (Ref. 19). As a result, the β transitions exhibit a much larger static-field Stark effect and the broadening of α, γ transitions is dominated by ion collisions rather than electron collisions near the arcjet exit plane. The two-photon absorption is an L_β transition, and, therefore, the theoretical tables should be reasonably accurate.

Stark broadening can be significant for the hydrogen atom even for electron density $\leq 10^{12}$ cm^{-3} because it is the most sensitive atom to Stark effects. Analysis of previous data on the H_α lineshape near the exit plane of an H_2 arcjet concluded that Stark broadening is large.[7] The effect of ion collisions with H atom dominates the Stark broadening under exit plane conditions, resulting in substantially greater broadening for some transitions, at plasma density $\leq 10^{15}$ cm^{-3}, than indicated in the standard theoretical compilations such as that by Vidal et al.[20]

The electron density was determined to be $6\text{–}10 \times 10^{13}$ cm^{-3} at the exit plane of the hydrogen arcjet at 1.4-kW input power, rapidly increasing with power level and rapidly decreasing with axial distance in the downstream direction.[7] Although the electron density of an arcjet operating on NH_3 propellant may be considerably higher in the arc than in the pure hydrogen case,[21] there appears to be no experimental evidence available that a significant difference persists at the exit plane for hydrogen and simulated hydrazine arcjets. At $n_e = 1 \times 10^{14}$ cm^{-3} the expected Stark lineshape of L_β at 2500 K is double peaked, with a sharp minimum at line center and FWHM $\sim$1.1 cm^{-1} at the one-photon L_β transition ($\Delta\nu/\nu_0 = 1.1 \times 10^{-5}$).

Not only does the lineshape broaden more than expected near the exit plane, the experimentally observed signal intensity peaks at $z = 0.8$ cm then drops quickly (see Fig. 5) in the downstream direction. From a physical standpoint, the H atom density is expected to rise in the upstream direction as a monotonic function. There are a number of reasons why the observed peak signal could decrease even as the density is increasing, including 1) Stark and Doppler broadening, 2) occlusion of fluorescence by the arcjet nozzle, 3) inaccurate alignment of laser/arcjet/fluorescence detection apparatus, 4) self-absorption or amplified spontaneous emission, 5) quenching effects, and 6) mixing of upper state wave functions by collisions and/or electric fields causing breakdown of selection rules and changes in fluorescence lifetime or fluorescence pathways.

The temperature does not change quickly enough for Doppler broadening to be a dominant factor, and Stark broadening does not appear to fit the observed lineshape; nor is the lineshape broadened sufficiently to explain the observed intensity drop near the exit plane. At a distance of 1 mm from the exit plane,

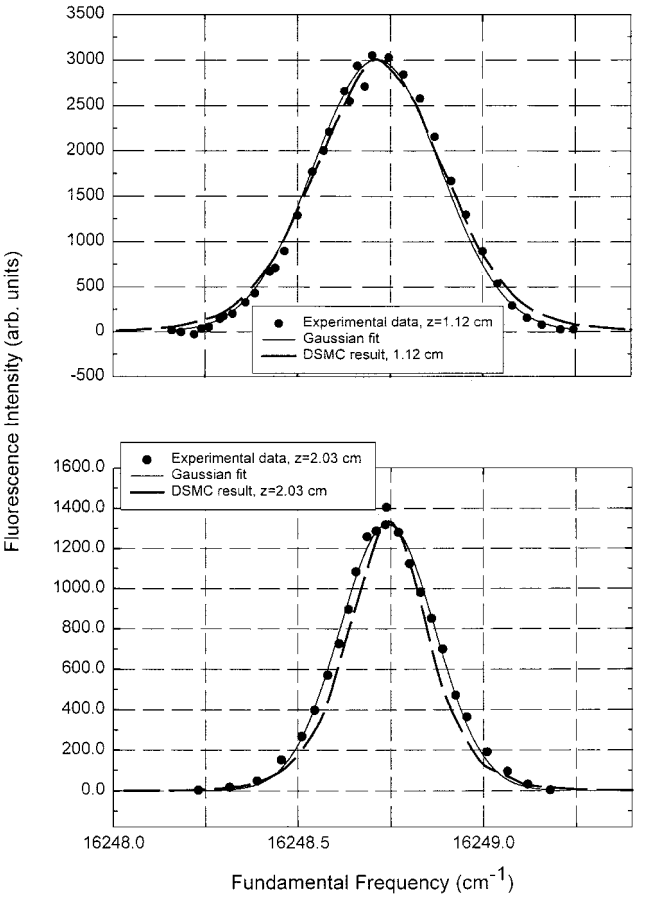

Fig. 3 Lineshapes on plume centerline at 11.2 (upper panel) and 20.3 (lower panel) ± 0.3 mm downstream from exit plane; laser beam intersected the plume perpendicular to the thrust axis.

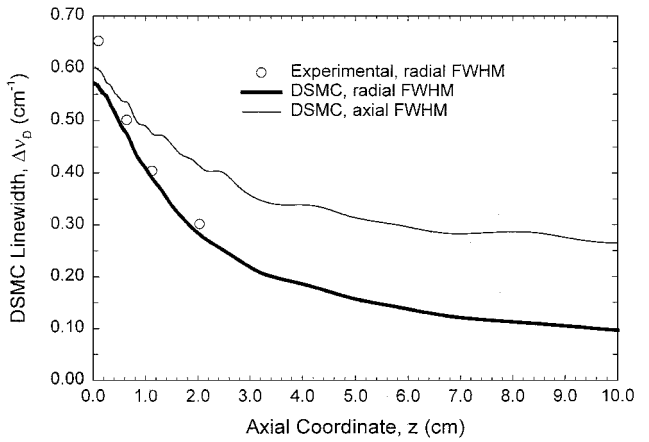

Fig. 4 Experimental and theoretical linewidths on centerline, for the fundamental laser frequency.

fluorescence occlusion is negligible, and the alignment accuracy of the laser/arcjet/fluorescence detection apparatus is certainly better than 1 mm. This leaves reasons 4–6 as potential explanations.

The decrease in fluorescence intensity due to the self-absorbing medium between probe volume and collection lens can be estimated from the relation

$$-\mathrm{d}I_\nu(x) = k_\nu I_\nu \,\mathrm{d}x \tag{10}$$

where the 8-deg divergence (half-angle) has been neglected. Upon integrating through the medium, the result is

$$I_\nu(L) = I_\nu(0)e^{-\bar{k}_\nu L} \tag{11}$$

where the further approximation has been made of replacing k_ν in the integral

$$-\int_0^L k_\nu \,\mathrm{d}x$$

by an effective (average) value over the distance L. When the relationship between transition oscillator strength and absorption coefficient is used:

$$\int k_\nu \,\mathrm{d}\nu = \frac{e^2}{4\varepsilon_0 mc} N_i f \tag{12}$$

the value of $\bar{k}_\nu L$ can be estimated.

The value of N_i in Eq. (12) is highly uncertain, and this quantity, therefore, determines the accuracy. Emission spectroscopy of medium power hydrogen arcjet plumes has measured H atom emission from many different levels and produced estimates of the number density.[22] At 6 kW, the number density of $n = 3$ at $z = 2.75$ mm was about 6×10^{10} cm^{-3}. Measurement of $n = 2$ number density was much more difficult because of the vacuum UV wavelength and because the plume is optically thick with respect to the Lyman series. The background power level that pumps the L_α transition is estimated to be on the order of 1 mW cm^{-2} near the exit plane[21] and may enhance $n = 2$ with respect to other excited states.

Starting from the Doppler-broadened Gaussian lineshape for $T = 2100$ K, about the value predicted by the DSMC calculation on-centerline for $z = 0.10$ cm, the modified lineshape was computed by choosing $\bar{k}_\nu L$ such that the FWHM agreed with the experimental data. The result is shown in Fig. 6. The new lineshape obtained by including self-broadening can reproduce the experimental lineshape very well, better than least-squares fitting to a pure Gaussian function. The value of $\bar{k}_\nu L$ needed was 0.45, corresponding to an average density of about 1×10^{12} cm^{-3} over a pathlength of 5 mm.

Amplified spontaneous emission (ASE) will preferentially reduce the fluorescence yield where H atom density is high. ASE production has been previously characterized and compared to fluorescence intensity for the same system of levels in the case of two-photon excitation.[6,23,24] Whereas LIF intensity has a quadratic dependence on laser intensity at low to moderate levels, ASE intensity has approximately a quartic dependence. The estimated diameter of the focused laser is 0.1 mm in the probed region. When compared to the data of Wysong and Pobst[6] obtained at about half the laser beam radius, LIF and ASE intensity will not be in the saturated regime. Although the effect of ASE on the lineshape is difficult to calculate accurately due to its nonlinearity, ASE is believed to be less compatible with the observed lineshape than self-absorption. In addition, fluorescence should be considerably more intense than ASE under the conditions of the measurements.[6,23,24] The effect of ASE on the observed signal intensity and linewidth was, therefore, assumed to be small in the present study, and no attempt was made to correct for it.

By the use of the relation

$$\Delta\nu \cong \sqrt{\Delta\nu_D^2 + \Delta\nu_l^2 + \Delta\nu_S^2 + \Delta\nu_{\mathrm{SA}}^2} \tag{13}$$

and Eqs. (6–9), the temperatures listed in Table 2 were obtained for each of the measured lineshapes of Figs. 2 and 3. The lineshape analysis is approximate, as already discussed. Error limits in all cases but $z = 0.10$ cm were based on the standard deviation of the fitted lineshape and uncertainty in the laser linewidth. No Stark or self-absorption corrections were made for these data points, just

Table 2 Hydrogen atom radial (perpendicular) translational temperatures

r, z, cm	FWHM at 1025 Å cm^{-1}	Temperature, K	Error limits, K
0, 0.10	3.91	2180[a]	±250
0, 0.64	2.99	1786	±150
0, 1.12	2.42	1204	±80
0, 2.03	1.81	670	±60

[a]DSMC result.

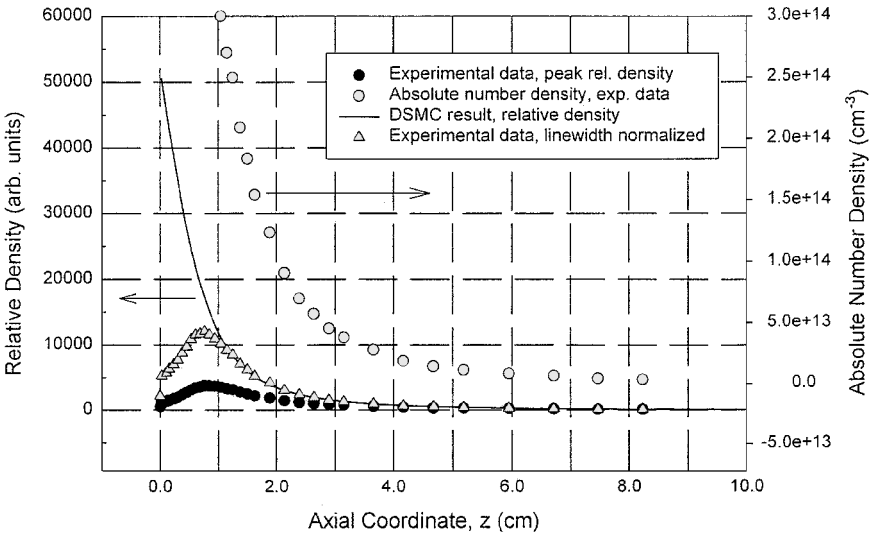

Fig. 5 Experimental and theoretical axial density profiles.

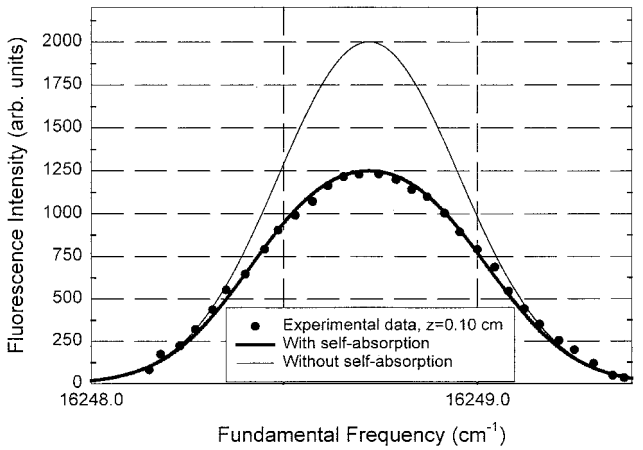

Fig. 6 Self-absorption broadening near the exit plane, comparing a pure 2100 K Gaussian with a broadened one.

as none were made in the previous two-photon LIF study of H lineshapes in the NASA 1-kW hydrogen arcjet.[6]

The experimental linewidth at $r = 0$ and $z = 0.10$ cm, corresponds to about 3150 K if due to Doppler broadening alone. This value is extremely high, given the relatively low DSMC prediction and the temperature of the nozzle wall, as well as previous results for the hydrogen arcjet. In view of the clear possibility that a non-Doppler mechanism was involved in broadening the lineshape, and the degree of success usually obtained by the DSMC method in predicting temperature, the DSMC result is considered to be a more accurate temperature indicator at this plume location. The DSMC temperature is, therefore, the one reported in Table 2.

An equivalent amount of Stark broadening requires several times higher plasma density than has been measured in the hydrogen arcjet and would produce a sharp minimum at the center of the lineshape. Self-absorption will produce a broad minimum at the line center when the absorption is strong and can account for part of the reduction in peak signal intensity near the exit plane. It is proposed that the lineshape near the exit plane was indeed broadened primarily by self-absorption. To the extent that Stark broadening has occurred, however, the degree of self-absorption will have been overestimated.

Quenching and Mixing Effects

The mixing or redistribution of upper state level populations occurs in the presence of electric fields and during collisions. The electric field near the arcjet exit plane may be too low to cause mixing. Based on modeling and experimental results for $n = 3$ H atoms populated through the $n = 3 \leftarrow n = 1$ two-photon absorption, just a few hundred millitorr of H_2 is sufficient to equilibrate the populations of the $n = 3$ angular momentum states, $L = 0-2$. The initial population distribution is about 12% S state and 88% D state as determined by the absorption cross sections (selection rules prohibit initial population of the P state). On equilibration, the populations become 11.1% S, 33.3% P, and 55.6% D, in accordance with the statistical weighting associated with level degeneracies. Because of the 159-ns lifetime of $3S$ and little change in its population, the $3S$ contribution to detected fluorescence can be neglected. In contrast, the population of $3P$ opens up two new fluorescence channels, $3P$–$2S$ and $3P$–$1S$, with a branching ratio of 0.118. Even the $3P$–$2S$ channel contributes little to the fluorescence signal, due to its 46-ns lifetime.

The quenching rate constants for $n = 3$ H atom are approximately 1.9×10^{-9} and 2.8×10^{-9} cm^3/s for H_2 and N_2, respectively.[25] With the assumed densities of 5×10^{15} and 2.5×10^{15} cm^{-3} for H_2 and N_2, respectively, the partial pressures are estimated to be 0.37 and 0.18 torr at the approximate plume temperature of 2000 K. When it is assumed that the quenching rates are proportional to pressure and independent of temperature or velocity,[26] use of the quantum yields from Table 2 of Ref. 25 indicates a combined quantum yield of 0.47 due to H_2 and N_2 quenching. The combined signal reduction factor from quenching and self-absorption is, therefore, estimated to be $(0.47)(1250/2000) = 0.29$ at the $z = 0.10$ cm location. After applying this correction and a further correction for the radial linewidth variation, the comparison of DSMC and experimental data at $z = 1.25$ cm and $z = 0.10$ cm leads to the conclusion that the observed signal at $z = 0.10$ cm is still low by a factor of 2. The reason for this is uncertain. One possible explanation relates to the reduced fluorescence lifetime near the exit plane and the use of a constant boxcar delay and gate width. Other possibilities include ASE, larger-than-calculated mean axial velocity at the exit plane, and higher quenching rates than anticipated.

Density and Velocity Distribution

The absolute H atom density was computed by extrapolating the mass spectrometer flux data at $z = 13$ cm to a density figure[27] and applying $1/z^2$ scaling to connect with LIF data at 8.2 cm, enabling generation of the absolute density plot of Fig. 5. Only this absolute density result applies to the right-hand Y axis of Fig. 5. Using the ratio of densities at $z = 0.0$ and 1.2 cm predicted by the DSMC results (these data are considered reliable in terms of relative density), a hydrogen atom density of 1.4×10^{15} cm^{-3} was computed at the exit plane, on the centerline. A slight underestimate might be expected due to the extrapolation from 13 to 8.2 cm and because the mass

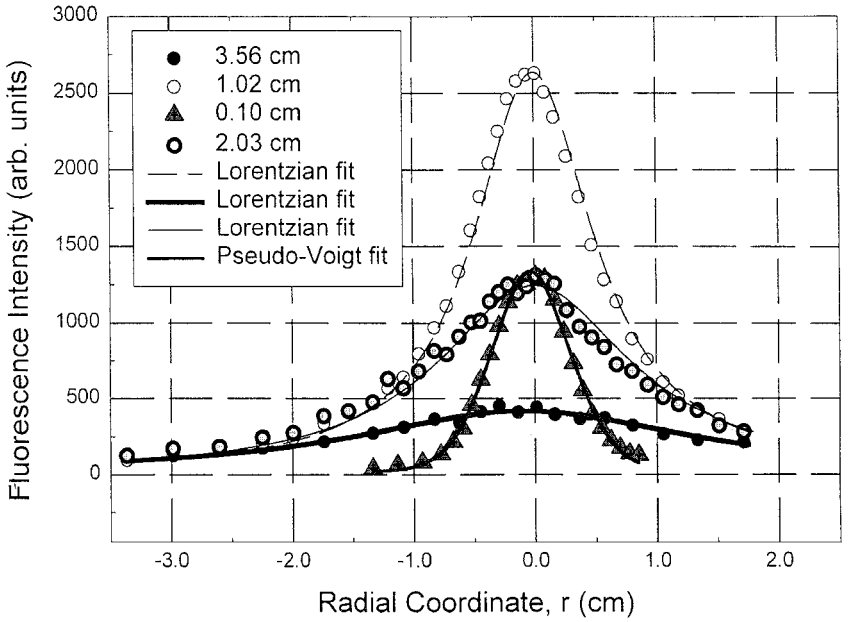

Fig. 7 Radial profiles of peak fluorescence intensity.

spectrometry detects only the atoms with virtually zero radial velocity. The absolute density of the KARNAC result was 5×10^{15} cm^{-3}. Because the mass spectrometry concluded that the H mole fraction was about 40% of the theoretical prediction, 2×10^{15} cm^{-3} is taken to be the absolute density of H atoms at the exit plane, on centerline, with absolute error estimated at $+50/-40\%$.

Radial peak signal profiles, essentially the fluorescence intensity along several radial cuts with laser frequency tuned to the center of the spectral transition, are plotted in Fig. 7. Lorentzian fits gave significantly better results than Gaussian fits in most cases, but near the exit plane ($z = 0.10$ cm) a combination of Lorentzian and Gaussian functions was needed for a good fit. It is expected that the radial density distribution will depend strongly on the radial velocity distribution function, which is presumed to be Gaussian all along the radial direction. (It was determined to be Gaussian on centerline; see Figs. 2 and 3.) Because of reduced temperature and lower quenching rates on the periphery of the plume, the tail of the radial density distribution will be enhanced. The use of a Lorentzian function, therefore, does not seem unreasonable, although it is highly unusual for the present problem of a radial density profile in an expanding plume. The alternative function $\cos^n\theta$, where θ is the angle with respect to the thrust axis and n is 3–5, although commonly used for this role, did not fit well in the present case.

Self-absorption of the magnitude described will produce a slight distortion of the radial profile at $z = 0.10$ cm (see Fig. 7). Fluorescence from the far side of the plume undergoes more self-absorption than on the near side, leading to an enhancement of signal on the near side and a shift in peak position of about 1 mm according to a simple model. The quenching effect will also distort the radial profile, producing a flattened peak. Whereas the $z = 0.10$ cm profile appears to exhibit a shift in peak position of 0.3 mm, the accuracy of the measurements does not permit a conclusive determination regarding the magnitude of a shift or of asymmetry in the radial profile, or even that such anomalies occurred.

Because of the position dependence of the width of the thermal velocity distribution, direct comparison of the radial peak density profile obtained with the probe laser positioned at the spectral line center could not be made to the DSMC radial density profile. The radial variation of the spectral linewidth was, therefore, determined from the dependence of the DSMC velocity distribution function on spatial coordinate and multiplied on a coordinate-by-coordinate basis with the experimental peak density to obtain the integrated relative density at each data point. Laser linewidth was assumed to be small, relative to spectral linewidth, for the purpose of this transformation. Figure 8 shows the radial density profiles obtained from this product of calculated thermal width and measured peak signal.

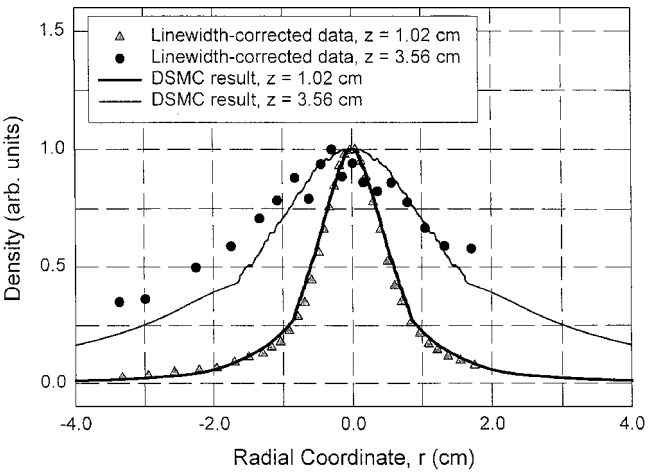

Fig. 8 Radial density profiles.

DSMC density profiles are included for comparison. The effect of multiplying the experimental data by the DSMC linewidths can be seen by comparing the profiles of Figs. 7 and 8. The $z = 1.02$ cm profile of Fig. 8 is more narrow than in Fig. 7 because the lower temperature on the periphery results in a smaller linewidth factor there. The opposite occurs for the $z = 3.56$ cm profile. In each case, the close agreement between the pure-theory profile and that derived by applying the DSMC linewidth factor to the experimental data strongly suggests that the theoretical results are accurate. The comparison at $z = 3.56$ cm is not as favorable as the $z = 1.02$ cm case, but the experimental data are noisy there and the profile is asymmetric. It is not clear whether theory or experiment is more accurate for radial cuts far from the nozzle exit plane.

The DSMC Doppler linewidth predictions used to generate Fig. 8 are plotted in Fig. 9, together with fitted curves. These results were monitored at several intervals during the computation, which was performed for a longer period than usual to further reduce statistical error. The variation in corresponding $\Delta\nu_D$ data points suggested that an error limit of several percent may apply to the end result, when it is assumed that all vital elements have been incorporated into the DSMC model and that the KARNAC results were appropriate. The estimated error limit in Table 2 for $\Delta\nu_D$, at $z = 0.10$ cm on centerline, was based on this and model validation results to date.

The shift of peak signal when the laser source traversed the plume at centerline, 1.2 cm from the exit plane at 39 deg with respect

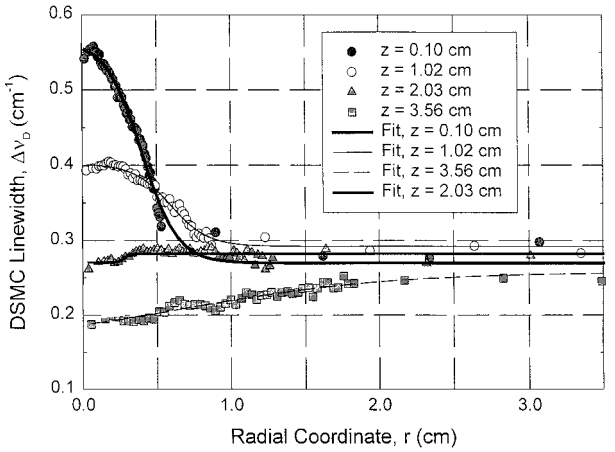

Fig. 9 DSMC radial linewidth results, for the fundamental laser frequency.

to plume axis, was consistent with an H atom axial velocity of 9.2 ± 1.3 km/s. Given the large error bar and just a single data point, validation of the corresponding DSMC result was not feasible. Because of alignment difficulties and time constraints, the peak velocity and axial velocity distributions were not pursued further.

Summary

Temperature, velocity, and relative density measurements of the hydrogen atom were obtained in the simulated hydrazine arcjet plume. As in the case of the NH molecule, comparisons between experimental and theoretical results were in generally good agreement for a flight-type hydrazine arcjet, demonstrating the utility of the DSMC code for applications beyond the hydrogen arcjet. Agreement between theory and experiment was very good for the radial density profiles. Close agreement was also obtained for lineshapes and the axial density profile, except near the exit plane, where the discrepancy can be large. Spatially dependent quenching and linewidth and velocity distribution broadening reduced the observed signal near the exit plane. In addition, self-absorption may have broadened the lineshape and further reduced the signal in that plume region.

A positive synergy between experiment and theory has been useful in furthering the fundamental understanding of the arcjet. A comprehensive picture is beginning to emerge regarding the atomic and molecular energy distribution for all available modes throughout the arcjet plume.

Acknowledgments

The original data were obtained under contract to MELCO (Mitsubishi Electric Corporation) during 1997–1998. Preparation of the manuscript, which used a 1998 report to MELCO as the starting point, was partially funded by the Aerospace IR&D program. Thruster operations support was provided by D. Zube, J. English, and S. Crook of PRIMEX Aerospace, and J. Pollard, M. Worshum, L. Ortega, and E. Fournier of The Aerospace Corporation. E. Beiting, J. Pollard, and R. Cohen provided valuable assistance in other aspects of the project. We also thank I. Wysong for a useful discussion. This work was presented as Paper 99-048 at the 26th International Electric Propulsion Conference, Kitakyushu, Japan, October 1999.

References

[1]Zube, D. M., Fye, D., Masuda, I., and Gotoh, Y., "Low Bus Voltage Hydrazine Arcjet System for Geostationary Satellites," AIAA Paper 98-3631, July 1998.

[2]Martinez-Sanchez, M., and Pollard, J. E., "Spacecraft Electric Propulsion," *Journal of Propulsion and Power*, Vol. 14, No. 5, 1998, pp. 688–699.

[3]Nelson, D. A., Gotoh, Y., and Masuda, I., "A Simplified Model for the Prediction of Arcjet Plumes," International Electric Propulsion Conf., IEPC Paper 99-043, Oct 1999.

[4]Pollard, J. E., "Arcjet Diagnostics by XUV Absorption Spectroscopy," AIAA Paper 92-2966, July 1992.

[5]Erwin, D. A., Pham-Van-Diep, G. C., and Deininger, W. D., "Laser-Induced-Fluorescence Measurements of Flow Velocity in High-Power Arcjet Thruster Plumes," *AIAA Journal*, Vol. 29, No. 8, 1991, pp. 1298–1303.

[6]Wysong, I. J., and Pobst, J. A., "Quantitative Two-Photon Laser-Induced Fluorescence of Hydrogen Atoms in a 1 kW Arcjet Thruster," *Applied Physics B*, Vol. 67, No. 2, 1998, pp.193–205.

[7]Storm, P. V., and Cappelli, M. A., "Stark Broadening Corrections to Laser-induced Fluorescence Temperature Measurements in a Hydrogen Arcjet Plume," *Applied Optics*, Vol. 35, No. 24, 1996, pp. 4913–4918.

[8]Crofton, M. W., Moore, T. A., Boyd, I. D., Masuda, I., and Gotoh, Y., "Near-Field Measurement and Modeling Results for Flight-Type Arcjet: NH Molecule," *Journal of Spacecraft and Rockets*, Vol. 38, No. 1, 2001, pp. 79–86.

[9]Smith, R. D., Roberts, C. R., Aadland, R. S., Lichtin, D. A., and Davies, K., "Flight Qualification of the 1.8 kW MR-509 Hydrazine Arcjet System," International Electric Propulsion Conf., IEPC Paper 97-081, Aug. 1997.

[10]Morren, W. E., and Lichon, P. J., "Low-Power Arcjet Test Facility Impacts," AIAA Paper 92-3532, July 1992.

[11]Kligler, D. J., and Rhodes, C. K., "Observation of Two-Photon Excitation of the H_2 E, F $^1\Sigma_g^+$ State," *Physical Review Letters*, Vol. 40, No. 5, 1978, pp. 309–313.

[12]Van Baak, D. A., Clark, B. O., and Pipkin, F. M., "The $3\,^2S_{1/2}$–$3\,^2D_{5/2}$ Interval in Atomic Hydrogen. I. Two-photon Line-shape Theory," *Physical Review A: General Physics*, Vol. 19, No. 2, 1979, pp. 787–801.

[13]Boyd, I. D., "Monte Carlo Simulation of Nonequilibrium Flow in Low Power Hydrogen Arcjets," *Physics of Fluids*, Vol. 9, No. 10, 1997, pp. 3086–3095.

[14]Butler, G. W., Boyd, I. D., and Cappelli, M. A., "Nonequilibrium Flow Phenomena in Low Power Hydrogen Arcjets," AIAA Paper 95-2819, July 1995.

[15]Bird, G. A., *Molecular Gas Dynamics and the Direct Simulation of Gas Flows*, Oxford Univ. Press, Oxford, 1994.

[16]Boyd, I. D., "Extensive Validation of a Monte Carlo Model for Hydrogen Arcjet Flowfields," *Journal of Propulsion and Power*, Vol. 13, No. 6, 1997, pp. 775–782.

[17]Verkerk, P., Pinard, M., Biraben, F., and Grynberg, G., "1S-3S and 1S-3D Doppler-Free Two-Photon Transition in Hydrogen and Deuterium," *Optics Communications*, Vol. 72, No. 3–4, 1989, pp. 202–204.

[18]Booth, J. P., Derouard, J., Fadlallah, M., Cabaret, L., and Pinard, J., "Electric Field Measurements in Discharges by Doppler-Free Two-Photon Laser Stark Spectroscopy of Atomic Hydrogen," *Optics Communications*, Vol. 132, No. 3–4, 1996, pp. 363–370.

[19]Kelleher, D. E., Wiese, W. L., Helbig, V., Greene, R. L., and Oza, D. H., "Advances in Plasma Broadening of Atomic Hydrogen," *Physica Scripta*, Vol. T47, 1993, pp. 75–79.

[20]Vidal, C. R., Cooper, J., and Smith, E. W., "Hydrogen Stark-Broadening Tables," *Astrophysical Journal Supplement Series*, Vol. 25, No. 214, 1973, pp. 37–136.

[21]Crofton, M. W., "Spectral Irradiance of the 1-kW Arcjet Thruster from 80 to 500 nm" AIAA Paper 92-3237, July 1992.

[22]Hoskins, W. A., Kull, A. E., and Butler, G. W., "Measurement of Population and Temperature Profiles in an Arcjet Plume," AIAA Paper 92-3240, July 1992.

[23]Amorim, J., Baravian, G., and Touzeau, M., "Two-photon Laser Induced Fluorescence and Amplified Spontaneous Emission Atom Concentration Measurements in O_2 and H_2 Discharges," *Journal of Applied Physics*, Vol. 76, No. 3, 1994, pp. 1487–1493.

[24]Goldsmith, J. E. M., "Two-photon-excited Stimulated Emission from Atomic Hydrogen in Flames," *Journal of the Optical Society of America B*, Vol. 6, No. 11, 1989, pp. 1979–85.

[25]Preppernau, B. L., Pearce, K., Tserepi, A., Wurzberg, E., and Miller, T. A., "Angular Momentum State Mixing and Quenching of $n = 3$ Atomic Hydrogen Fluorescence," *Chemical Physics*, Vol. 196, No. 1–2, 1995, pp. 371–381.

[26]Terezawa, N., Ukai, M., Kouchi, N., Kameta, K., and Hatano, Y., "De-excitation of H (2p) in a Collision with a H_2 Molecule," *Journal of Chemical Physics*, Vol. 99, No. 3, 1993, pp. 1637–1643.

[27]Pollard, J. E., Masuda, I., and Gotoh, Y., "Plume Mass Spectrometry with a Hydrazine Arcjet Thruster," *Journal of Spacecraft and Rockets*, Vol. 38, No. 3, 2001, pp. 411–416; also International Electric Propulsion Conf., IEPC Paper 99-041, Oct. 1999.

A. Ketsdever
Guest Associate Editor